Permeability for Flow of Interdendritic Liquid in Columnar-Dendritic Alloys

D. R. POIRIER

Permeability data for the flow of interdendritic liquid in partially solid Pb-Sn and borneol-paraffin columnar-alloys are summarized. The data are used in regression analyses and simple flow models to arrive at relationships between permeability and the morphology of the solid dendrites. When flow is parallel to the primary dendrite arms, the important morphological aspects are the volume fraction liquid (g_L) and the primary dendrite arm spacing (d_1). When flow is normal to the primary dendrite arms, the permeability depends upon the secondary dendrite arm spacing (d_2) as well as d_1 and g_L. The parallel permeability is best described by a model based on the Hagen-Poiseuille law for laminar flow through a tube; for the normal permeability an empirical multilinear regression gives the best fit to the data. However, those models are not appropriate for extrapolations beyond the range of the available data ($0.19 \leq g_L \leq 0.66$), particularly as g_L approaches 1. For extrapolations, models based upon the Blake-Kozeny equation for flow through porous media are recommended.

I. INTRODUCTION

IT is well known that the convection of interdendritic liquid in solidifying alloys is responsible for many types of macrosegregation. To model the convection and hence macrosegregation, D'Arcy's law is used. When inertial effects are negligible, D'Arcy's law is written as

$$\mathbf{v} = -(K/\mu g_L)(\nabla P - \rho \mathbf{g}) \quad [1]$$

where $\mathbf{v}$ = velocity of the interdendritic liquid, $m \cdot s^{-1}$
μ = viscosity of the interdendritic liquid, $N \cdot s \cdot m^{-2}$
g_L = volume fraction of the interdendritic liquid
P = pressure, $N \cdot m^{-2}$
ρ = density of the interdendritic liquid, $kg \cdot m^{-3}$
$\mathbf{g}$ = gravitational acceleration, $m \cdot s^{-2}$

and

K = specific permeability of the solid-liquid zone, m^2.

Obviously the specific permeability is a key parameter in modeling of macrosegregation; yet there are relatively few data available.

Permeabilities in equiaxial dendritic structures have been reported by Piwonka and Flemings,[1] Apelian *et al.*,[2] Streat and Weinberg,[3] Takahashi *et al.*,[4] and Murakami and Okamoto.[5] Permeabilities in columnar dendritic structures have been reported by Streat and Weinberg,[3] Murakami *et al.*,[7,8] and Nasser-Rafi *et al.*[6] Some of these works have been discussed in a previous paper,[6] with particular emphasis given to experimental techniques. Here the purpose is to analyze and discuss the permeability for columnar structures, so permeability data for flow in equiaxial structures are not considered further.

Because of the directional nature of a columnar-dendritic structure, its permeability is anisotropic.[6,7,8] Here the principal flow directions are selected to be parallel and normal to the primary dendrite arms, then the components of the permeability are K_y and K_x, respectively. Accordingly, the components of Eq. [1] are

$$v_y = -(K_y/\mu g_L)(\partial P/\partial y - \rho g_y) \quad [2]$$

and

$$v_x = -(K_x/\mu g_L)(\partial P/\partial x - \rho g_x) \quad [3]$$

where v_x, v_y = velocity components in the x and y directions, respectively.

and

g_x, g_y = components of $\mathbf{g}$.

Data illustrating this anisotropy of permeability in columnar structures were presented by Murakami *et al.*[7,8] for borneol-paraffin organics which have a dendritic morphology the same as that of metallic alloys. More recently, Nasser-Rafi *et al.*[6] considered the anisotropic permeability in Pb-20 wt pct Sn columnar alloys. Here we reexamine the data from those three works,[6,7,8] along with those of Streat and Weinberg,[3] and include additional results which have been obtained for Pn-20 wt pct Sn alloys. The collective data are analyzed by empirical regression analyses and by physical models, some of which have been previously used to represent permeability in porous media.

II. PERMEABILITY DATA FOR COLUMNAR-DENDRITIC STRUCTURES

Summaries of the data for permeability when flow is parallel to and normal to the primary dendrite arms are given in Tables I and II, respectively.

The data listed in Tables I and II that are attributed to Streat and Weinberg[3] have "SW" designations, and those from Murakami *et al.*[7,8] have "M" designations. As those data appear in Tables I and II, they can also be found in the original references. However, the data from Nasser-Rafi *et al.*[6] (designations "RN") have been modified somewhat as discussed below. The additional data (designations "RI") were obtained using procedures similar to those described previously.[6]

The permeameter shown in Figure 1 is a modified version of that shown as Figure 6 in Nasser-Rafi *et al.*[6] Test specimens were cut from Pb-20 wt pct Sn ingots with directional-columnar structures and visually examined to ascertain that no "freckles" existed. The specimens were carefully machined in order to fit very snugly in the permeameter; these were 40 mm wide, 9 mm thick and varied in vertical height

D. R. POIRIER is Professor, Department of Materials Science and Engineering, The University of Arizona, Tucson, AZ 85721.

Manuscript submitted June 23, 1986.

Table I. Permeability for Flow Parallel to Primary Dendrite Arms

Designations	d_1, μm	d_2, μm	g_L	K, m^2	System	Reference
RI-22	185	68	0.2038	1.66×10^{-12}	Pb-20 wt pct Sn	this work
RI-23	221	68	0.1742	1.80×10^{-12}	Pb-20 wt pct Sn	this work
RI-24	275	84	0.1875	2.40×10^{-12}	Pb-20 wt pct Sn	this work
RI-26	297	91	0.1904	2.02×10^{-12}	Pb-20 wt pct Sn	this work
RI-27	155	54	0.2022	3.69×10^{-13}	Pb-20 wt pct Sn	this work
RI-28	171	62	0.2089	1.48×10^{-12}	Pb-20 wt pct Sn	this work
RI-30	168	62	0.1771	8.76×10^{-13}	Pb-20 wt pct Sn	this work
RN-G	96	41	0.1887	8.34×10^{-14}	Pb-20 wt pct Sn	6
RN-B	113	48	0.1940	1.60×10^{-13}	Pb-20 wt pct Sn	6
RN-AJJ	141	51	0.1978	2.14×10^{-13}	Pb-20 wt pct Sn	6
RN-F1	169	59	0.2042	3.93×10^{-13}	Pb-20 wt pct Sn	6
RN-M	187	60	0.2064	5.65×10^{-13}	Pb-20 wt pct Sn	6
RN-D	118	52	0.2900	2.20×10^{-13}	Pb-20 wt pct Sn	6
RN-Y1	129	48	0.2853	3.62×10^{-13}	Pb-20 wt pct Sn	6
RN-AJ	152	50	0.2898	6.56×10^{-13}	Pb-20 wt pct Sn	6
RN-F2	182	61	0.2860	1.41×10^{-12}	Pb-20 wt pct Sn	6
SW1	28	23	0.1900	1.10×10^{-14}	Pb-20 wt pct Sn	3
SW2	28	23	0.1900	2.00×10^{-14}	Pb-20 wt pct Sn	3
SW3	28	23	0.1900	1.50×10^{-14}	Pb-20 wt pct Sn	3
SW4	28	23	0.1900	2.40×10^{-14}	Pb-20 wt pct Sn	3
SW5	28	23	0.1900	1.60×10^{-14}	Pb-20 wt pct Sn	3
SW6	28	23	0.1900	1.40×10^{-14}	Pb-20 wt pct Sn	3
SW7	51	33	0.1900	2.40×10^{-14}	Pb-20 wt pct Sn	3
SW8	51	33	0.1900	3.50×10^{-14}	Pb-20 wt pct Sn	3
SW9	51	33	0.1900	3.60×10^{-14}	Pb-20 wt pct Sn	3
SW10	51	33	0.1900	4.10×10^{-14}	Pb-20 wt pct Sn	3
SW11	51	33	0.1900	4.30×10^{-14}	Pb-20 wt pct Sn	3
SW12	70	46	0.1900	5.00×10^{-14}	Pb-20 wt pct Sn	3
SW13	70	46	0.1900	8.20×10^{-14}	Pb-20 wt pct Sn	3
SW14	81	55	0.1900	5.50×10^{-14}	Pb-20 wt pct Sn	3
SW15	81	55	0.1900	7.90×10^{-14}	Pb-20 wt pct Sn	3
SW16	81	55	0.1900	1.10×10^{-13}	Pb-20 wt pct Sn	3
SW17	116	55	0.1900	2.10×10^{-13}	Pb-20 wt pct Sn	3
SW18	160	80	0.1900	6.20×10^{-13}	Pb-20 wt pct Sn	3
SW19	160	80	0.1900	8.20×10^{-13}	Pb-20 wt pct Sn	3
M1	420	115	0.3740	8.90×10^{-12}	borneol-paraffin	8
M2	420	115	0.4340	1.00×10^{-11}	borneol-paraffin	8
M3	420	115	0.3930	7.20×10^{-12}	borneol-paraffin	8
M4	420	115	0.3720	6.50×10^{-12}	borneol-paraffin	8
M5	420	115	0.2840	4.10×10^{-12}	borneol-paraffin	8
M6	420	115	0.4980	1.50×10^{-11}	borneol-paraffin	8
M7	320	90	0.5250	1.30×10^{-11}	borneol-paraffin	8
M8	320	90	0.2770	1.80×10^{-12}	borneol-paraffin	8
M9	320	90	0.4960	1.30×10^{-11}	borneol-paraffin	8
M10	320	90	0.4030	7.20×10^{-12}	borneol-paraffin	8
M11	320	90	0.4070	7.80×10^{-12}	borneol-paraffin	8
M12	320	90	0.3970	5.60×10^{-12}	borneol-paraffin	8
M13	320	90	0.5000	1.10×10^{-11}	borneol-paraffin	8
M14	320	90	0.3800	5.30×10^{-12}	borneol-paraffin	8
M15	320	90	0.3390	3.30×10^{-12}	borneol-paraffin	8
M16	320	90	0.4270	1.00×10^{-11}	borneol-paraffin	8
M17	320	90	0.4270	9.00×10^{-12}	borneol-paraffin	8
M18	320	90	0.5180	1.80×10^{-11}	borneol-paraffin	8
M19	320	90	0.5180	2.00×10^{-11}	borneol-paraffin	8
M20	320	90	0.5000	1.70×10^{-11}	borneol-paraffin	8
M21	320	90	0.4860	2.10×10^{-11}	borneol-paraffin	8
M22	320	90	0.4830	2.00×10^{-11}	borneol-paraffin	8
M23	420	90	0.5240	3.10×10^{-11}	borneol-paraffin	8
M24	420	90	0.3910	1.10×10^{-11}	borneol-paraffin	8
M25	420	90	0.4960	2.20×10^{-11}	borneol-paraffin	8
M26	420	90	0.3350	9.90×10^{-12}	borneol-paraffin	8
M27	420	90	0.5170	2.80×10^{-11}	borneol-paraffin	8
M28	420	90	0.2700	4.50×10^{-12}	borneol-paraffin	8
M29	420	90	0.4220	1.80×10^{-11}	borneol-paraffin	8
M30	420	90	0.3950	1.10×10^{-11}	borneol-paraffin	8
M31	420	90	0.3990	1.20×10^{-11}	borneol-paraffin	8
M32	420	90	0.6060	6.20×10^{-11}	borneol-paraffin	8

Table II. Permeability for Flow Normal to Primary Dendrite Arms

Designations	d_1, μm	d_2, μm	g_L	K, m^2	System	Reference
RI-3	196	67	0.195	0.454×10^{-12}	Pb-20 wt pct Sn	this work
RI-12	235	76	0.192	0.263×10^{-12}	Pb-20 wt pct Sn	this work
RI-13	209	77	0.262	0.180×10^{-11}	Pb-20 wt pct Sn	this work
RI-14	261	84	0.216	0.263×10^{-12}	Pb-20 wt pct Sn	this work
RI-15	264	86	0.226	0.518×10^{-12}	Pb-20 wt pct Sn	this work
RI-16	230	81	0.216	0.150×10^{-12}	Pb-20 wt pct Sn	this work
RI-18	151	69	0.221	0.826×10^{-13}	Pb-20 wt pct Sn	this work
RI-19	292	98	0.205	0.646×10^{-12}	Pb-20 wt pct Sn	this work
RI-20	144	67	0.310	0.154×10^{-11}	Pb-20 wt pct Sn	this work
RI-31	286	107	0.283	0.409×10^{-11}	Pb-20 wt pct Sn	this work
RN-DD	106	39	0.197	0.516×10^{-14}	Pb-20 wt pct Sn	6
RN-Y2	118	45	0.199	0.892×10^{-14}	Pb-20 wt pct Sn	6
RN-JJ	146	44	0.193	0.327×10^{-13}	Pb-20 wt pct Sn	6
RN-F3	171	57	0.206	0.804×10^{-13}	Pb-20 wt pct Sn	6
M-N1	420	115	0.374	0.169×10^{-10}	borneol-paraffin	7
M-N2	420	115	0.534	0.380×10^{-10}	borneol-paraffin	7
M-N3	420	115	0.630	0.534×10^{-10}	borneol-paraffin	7
M-N4	420	115	0.268	0.425×10^{-11}	borneol-paraffin	7
M-N5	420	115	0.374	0.973×10^{-11}	borneol-paraffin	7
M-N6	420	115	0.441	0.178×10^{-10}	borneol-paraffin	7
M-N7	420	115	0.397	0.115×10^{-10}	borneol-paraffin	7
M-N8	420	115	0.503	0.195×10^{-10}	borneol-paraffin	7
M-N9	420	115	0.609	0.429×10^{-10}	borneol-paraffin	7
M-N10	420	115	0.272	0.347×10^{-11}	borneol-paraffin	7
M-N11	320	90	0.496	0.134×10^{-10}	borneol-paraffin	7
M-N12	320	90	0.407	0.303×10^{-11}	borneol-paraffin	7
M-N13	320	90	0.539	0.145×10^{-10}	borneol-paraffin	7
M-N14	320	90	0.604	0.229×10^{-10}	borneol-paraffin	7
M-N15	320	90	0.624	0.255×10^{-10}	borneol-paraffin	7
M-N16	320	90	0.282	0.152×10^{-11}	borneol-paraffin	7
M-N17	320	90	0.494	0.119×10^{-10}	borneol-paraffin	7
M-N18	320	90	0.422	0.472×10^{-11}	borneol-paraffin	7
M-N19	420	90	0.539	0.144×10^{-10}	borneol-paraffin	8
M-N20	420	90	0.274	0.224×10^{-11}	borneol-paraffin	8
M-N21	420	90	0.407	0.706×10^{-11}	borneol-paraffin	8
M-N22	420	90	0.375	0.664×10^{-11}	borneol-paraffin	8
M-N23	420	90	0.258	0.184×10^{-11}	borneol-paraffin	8
M-N24	420	90	0.616	0.300×10^{-10}	borneol-paraffin	8
M-N25	420	90	0.532	0.148×10^{-10}	borneol-paraffin	8
M-N26	420	90	0.372	0.611×10^{-11}	borneol-paraffin	8
M-N27	420	90	0.490	0.152×10^{-10}	borneol-paraffin	8
M-N28	420	90	0.658	0.348×10^{-10}	borneol-paraffin	8
M-N29	420	90	0.320	0.392×10^{-11}	borneol-paraffin	8

from approximately 40 to 80 mm. Above and below the test specimens were the so-called "liquid" portions which had a composition equal to that of the interdendritic liquid at the test temperature. To promote the penetration of the liquid into the partially melted test specimen, a thin layer of non-activated, rosin-base flux was brushed onto the mating surfaces and allowed to dry. The permeameter and its contents were then assembled with a glass cover-plate which was sealed with a thin layer of silicone rubber. Then the assembly was heated in an oven, which was equipped with forced convection to maintain a uniform temperature and with a controller capable of maintaining a "set point" temperature within ±0.5 °C.

The period required to achieve test temperature (222 °C to 250 °C) from room temperature was approximately 45 minutes. The tests were initiated after the liquid portion was at test temperature for 15 minutes, as measured with the chromel-alumel thermocouple inserted directly into the liquid portion above the test specimen. The threaded rod shown in Figure 1 served two purposes: first, it acted as a valve to prevent flow of metal up the channel until such time that the experiment was ready to begin; second, it was used as a height sensor as liquid slowly filled the channel. The bottom of the rod was tapered almost to a point, and it was used to contact the top of the liquid metal; in turn this activated the buzzer so that height *vs* time could be recorded. The height was determined simply by counting rotations and knowing the pitch of the screw. At the end of each test the permeameter was quenched in water.

The values of volume fraction of liquid, g_L, in Tables I and II were determined by measuring the volume fraction of eutectic constituent, and from that measurement calculation for the volume fraction of liquid at test temperature was done. The calculation to accomplish this was presented in the Appendix of a previous publication.[6] For the data presented for the first time, designation "RI" in Tables I and

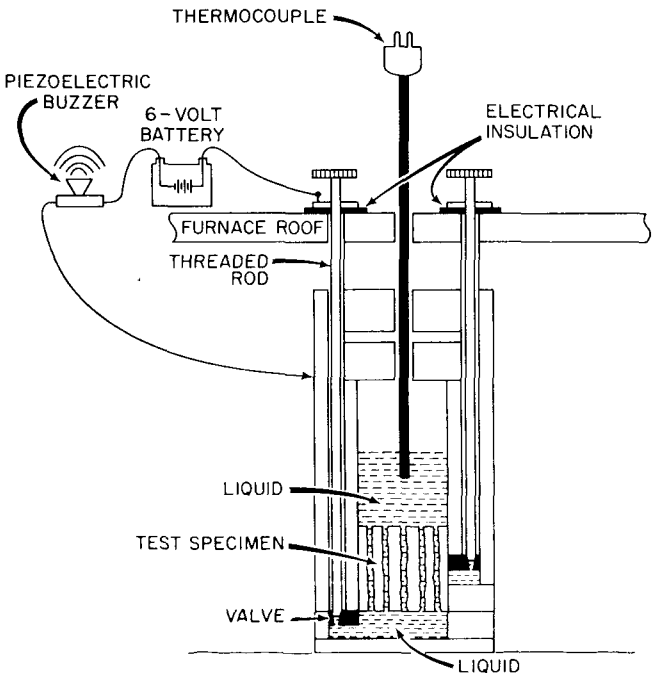

Fig. 1—The permeameter used to obtain data with designations RI in Tables I and II. For these data the valve on the right side was maintained in the closed position.

II, the volume fraction of the eutectic constituent was determined by point counting in an automated image-analyzer. Twenty-five fields at a magnification of 200× were surveyed for each specimen. By repeating the analyses for many specimens at several different "detect-levels", the results were always reproducible to within 0.5 pct of the volume fraction eutectic.

For specimen RI-20 the automated image-analyzer was not available. In this case a transparent grid of 400 points was placed over two photomicrographs, four times each, and the fraction of the total number of points which overlayed the eutectic constituent was taken to be the volume fraction of eutectic. Using the statistics given by Abrams,[9] the error, for a 95 pct confidence level, in the volume fraction of eutectic was 0.013. The volume fraction liquid was determined before and after each test; the values reported for designations RI and RN in Tables I and II are the simple arithmetic average.

Secondary dendrite arm spacings were also monitored by measurement on photomicrographs of samples from the test specimens before and after testing. Ripening of the dendritic structure did occur and the secondary dendrite arm spacings (d_2), shown in Tables I and II for the test specimens with the designations RI and RN, are interpolated values based upon the value of d_2 before and after the test and assuming that the variation of d_2 with time was as log d_2 with log t where t was the time that the test specimen existed in the solid plus liquid condition prior to and during the period when the permeability was determined. As discussed in previous works,[3,5-8] there is a flow period when the permeability is relatively constant, and after which the permeability varies. The mid-time of this period was considered to be the appropriate time to use for interpolating for d_2.

Chronologically the tests designated as RN preceded those designated as RI. In the earlier series of tests, it was assumed that the primary dendrite arm spacing would not change, so d_1 was measured only prior to the test. However, for the RI-series, d_1 was measured before and after the test, and a change of approximately 5 to 20 pct was consistently measured. The values of d_1 shown in Tables I and II for designation RI are, therefore, values interpolated in a manner similar to the interpolations for d_2. On the other hand, d_1 values for the RN designation are extrapolated values based upon the initial value of d_1 and assuming that d_1 varied with time according to

$$dd_1/dt = a/d_1^n \quad [4]$$

where a and n are constants. These constants were determined from the series RI in which d_1 was measured before and after the test and applying Eq. [4] in an approximate form:

$$\frac{\Delta d_1}{\Delta t} = a/\bar{d}_1^n \quad [5]$$

where Δd_1 = change in d_1 for total time Δt and $\bar{d}_1$ is the simple arithmetic average of d_1 before and after the test. Because the change in d_1 was relatively small (less than 20 pct), Eq. [5] is a good approximation to Eq. [4], so with a set of values of $(\Delta d_1/\Delta t)$ along with corresponding values of $\bar{d}_1$ a linear regression analysis was done to compute a and n.

In this work, d_1 was determined by counting the number of primary dendrite arms in photomicrographs (50× and 100× magnification) of prepared surfaces which were perpendicular to the primary dendrite arms. Thus the familiar "cruciforms" were counted, and then the primary dendrite arm spacing was calculated according to

$$d_1 = (A/N)^{1/2}$$

where N/A is the number of cruciforms per unit area.

Finally, it should be pointed out that the volume fractions of liquid reported for specimens with designations RN differ slightly from the values reported previously.[6] The differences are due to revising values of the densities used in calculating the volume fraction liquid at test temperature from a measured value of the volume fraction of eutectic at ambient temperature.

III. FLOW PARALLEL TO THE PRIMARY DENDRITE ARMS

A. *Multilinear Regression*

Here it is presumed that the permeability depends upon the volume fraction of interdendritic liquid, g_L, and the morphology of the dendrites as expressed in terms of the primary (d_1) and secondary (d_2) dendrite arm spacings. Following Murakami *et al.*,[8] the relationship among these variables is assumed to be

$$K = C d_1^p d_2^q g_L^r \quad [6]$$

where C, p, q, and r are constants which are determined by a multilinear regression on experimental data. The multilinear regression was done using available software[10] run on IBM-PC and IBM-PC/AT computers.

The results of "fitting" all data for parallel flow with Eq. [6] are shown in Figure 2. It is apparent that the data for

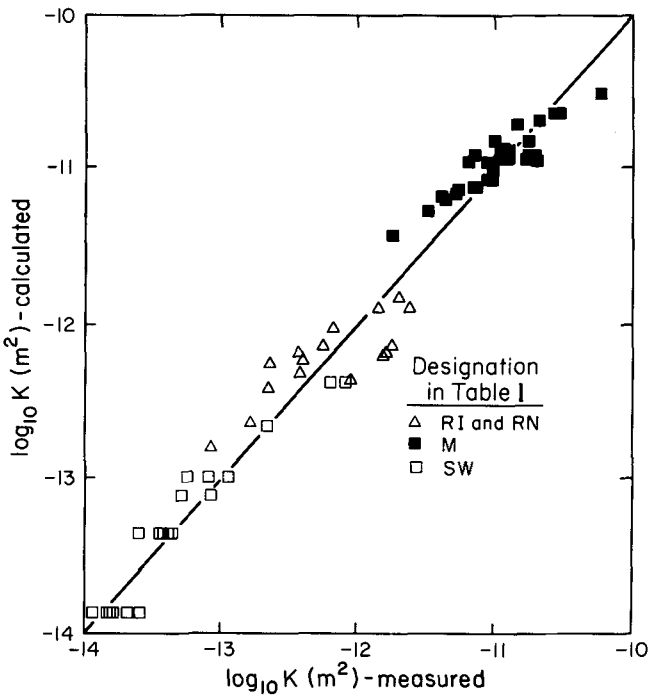

Fig. 2—Measured and calculated permeabilities, Eq. [7], for flow parallel to primary dendrite arms.

the borneol-paraffin series show little scatter when compared to the data for the Pb-Sn alloys; however, they extend over less than two decades for the value of K. By combining the Pb-Sn data and the borneol-paraffin data, a larger data set can be made, and the results apply to four decades for $\log_{10} K$ with a sample index of correlation equal to 0.98.

To construct Figure 2, the multilinear regression gave

$$K = 5.86 \times 10^{-16} d_1^{2.18} d_2^{-0.282} g_L^{1.98} \quad (\pm 37 \text{ pct}) \quad [7]$$

with K in m^2 and d_1 and d_2 in μm. The percentage in the parentheses is used as a figure of merit. It is the average percent deviation for the entire set where the percent deviation for each point is defined as

$$\text{Pct Deviation} = \left| \frac{K \text{ (measured)} - K \text{ (calculated)}}{K \text{ (measured)}} \right| \times 100 \quad [8]$$

Equation [7] does not compare well with that given by Murakami *et al.*[8] for their 32 data; their result is

$$K = 6.2 \times 10^{-13} d_1^{2.2} d_2^{-1.7} g_L^{3.2} \quad (\pm 29 \text{ pct}) \quad [9]$$

with K in m^2 and d_1 and d_2 in μm. The exponents have been verified, but the coefficient should be 8.98×10^{-13} which reduces the average deviation of their data to 18 pct. A major difference between Eqs. [7] and [9] is the exponent for d_2. Equation [7] indicates that K is slightly dependent on d_2 ($q = -0.282$), whereas Eq. [9] indicates a strong dependency ($q = -1.7$).

Murakami *et al.*[8] explained their results of decreasing permeability with an increasing d_2 by attributing it "to thickening of the secondary arms and therefore, to the reduction in the sectional area of each of the interdendritic channels." This explanation is plausible, but its validity depends upon the value of the exponent assigned to d_2. We believe that the permeability for flow parallel to the primary dendrite arms depends hardly, if at all, upon the secondary dendrite arm spacing. Nasser-Rafi *et al.*[6] compared their results to those of Streat and Weinberg[3] and showed equivalent permeabilities for equivalent primary dendrite arm spacings regardless of the secondary arm spacings. It should also be noted that the data of Murakami *et al.*[8] include only two values of d_2.

To add to our contention that K does not depend upon d_2, a multilinear regression was applied to the data of Murakami *et al.*[8] in which $q = 0$. The result is

$$K = 5.48 \times 10^{-15} d_1^{1.77} g_L^{3.32} \quad (\pm 20 \text{ pct}) \quad [10]$$

which gives a lesser average deviation from their experimental results than does Eq. [8], and with a comparable average deviation obtained by us for their data. Thus there is no compelling reason to assume that K depends on d_2. Extending the same reasoning to the set comprising the borneol-paraffin data and the Pb-Sn data, the result is

$$K = 4.15 \times 10^{-16} d_1^{2.02} g_L^{2.00} \quad (\pm 36 \text{ pct}) \quad [11]$$

with K in m^2 and d_1 and d_2 in μm. Notice that the average deviation is almost the same as that for Eq. [7]. On the other hand, if the exponent for d_1 is taken to be zero, then the average deviation is 53 pct. All of this indicates that the best equation to use, based upon the multilinear regression, is Eq. [11], particularly because it is also similar to a result based upon a physical model, the Hagen-Poiseuille law, as discussed below.

B. *Hagen-Poiseuille Model*

The Hagen-Poiseuille law gives the velocity of an incompressible fluid as it flows through a tube. It applies for fully-developed, laminar flow; in terms of the velocity, v, it is

$$v = -\frac{R^2}{8\mu}\left(\frac{dP}{dy} - \rho g\right) \quad [12]$$

where the flow is the direction of gravity (the y-direction)[11] and R is the tube radius.

For application to flow of interdendritic liquid parallel to the primary dendrite arms, envision a flow channel among the nearest neighbors of a set of primary dendrite arms; thus there is one flow channel per primary dendrite arm. The total volume flow rate through a partially solid alloy with a uniform g_L is

$$Q = vAg_L \quad [13]$$

where A is the total cross-sectional area of the solid-liquid zone, normal to the flow. Also, if each flow channel has an area of πR^2, then

$$Q = n\pi R^2 v \quad [14]$$

so that

$$R^2 = \pi^{-1} g_L (n/A)^{-1} \quad [15]$$

and n/A is simply the number of primary dendrite arms per unit area. The primary dendrite arm spacing, d_1, is

$$d_1 = \left(\frac{n}{A}\right)^{-1/2} \quad [16]$$

so that by combining Eqs. [12], [15], and [16] we have

$$v = -\left(\frac{1}{8\pi}\right)\frac{g_L d_1^2}{\mu}\left(\frac{dP}{dy} - \rho g\right). \quad [17]$$

D'Arcy's law for the same dendritic zone is

$$v = -\frac{K}{\mu g_L}\left(\frac{dP}{dy} - \rho g\right). \quad [18]$$

Hence by comparing Eqs. [17] and [18], the permeability is

$$K = C_1 d_1^2 g_L^2, \quad [19]$$

where C_1 is a parameter which depends upon the geometry of the flow channels. It could also include a tortuosity factor; even so the form of Eq. [19] would remain the same.

Equation [19] is similar in form to Eq. [11], if the exponent in Eq. [11] is adjusted slightly. If the same set of 67 data are used, then with $p = 2$

$$K = 3.75 \times 10^{-4} g_L^2 d_1^2 \quad (\pm 31 \text{ pct}) \quad [20]$$

where K and d_1^2 are in m^2. Notice that the multilinear regression has given Eq. [11], which is comparable to the result obtained by simply assuming that the Hagen-Poiseuille law applies. Equation [20] is preferred because it has a physical basis.

C. *Blake-Kozeny Model*

The Blake-Kozeny equation is used to describe slow flow through porous media. For flow in the vertical direction, it can be written as[12]

$$v = -C_2\frac{D^2 g_L^3}{\mu(1 - g_L)^2}\left(\frac{dP}{dy} - \rho g\right) \quad [21]$$

where C_2 = constant, v is the velocity within the interstices, and D is a characteristic dimension of the solid phase. For a packed bed of uniform spheres, D is the sphere diameter. For other shapes a shape factor is often applied, so D in Eq. [21] is replaced by D/λ with the net result of changing the value of C_2. Thus, Eq. [21] can be applied, without introducing λ, provided that the value of C_2 is considered to be dependent on the morphology of the solid phase.

By comparing Eqs. [18] and [21], the permeability is

$$K = C_2\frac{D^2 g_L^3}{(1 - g_L)^2}. \quad [22]$$

It is reasonable to assume that the characteristic dimension is related to the volume fraction of liquid by

$$1 - g_L \propto (D/d_1)^2. \quad [23]$$

Thus for $g_L = 0$, $D = 0$, and $K = 0$; for $g_L = 1$, $D = d_1$ and $K \to \infty$. Equation [23] also implies that the space among nearest primary dendrite arms is the location of a flow channel (as in the Hagen-Poiseuille model). Then by combining Eqs. [22] and [23], there results

$$K = C_2\frac{d_1^2 g_L^3}{(1 - g_L)}. \quad [24]$$

Using the borneol-paraffin data and the Pb-Sn data of Table I and expressing K and d_1^2 in m^2, the average value of C_2 is 1.43×10^{-3} and the average deviation is 92.0 pct.

The average deviation for the set of 67 data can be reduced significantly if it is assumed that C_2 depends upon the volume fraction of liquid, g_L. As the volume fraction of liquid decreases the dendritic solid becomes increasingly consolidated, so that from this change in morphology of the solid-phase the value of C_2 would be expected to increase with decreasing g_L. This behavior can be seen in Figure 3, where C_2 is plotted *vs* g_L. The curve shown in Figure 3 is based upon a one-dimensional, least squares regression for three parameters.[10] The result of that regression is

$$C_2 = 4.53 \times 10^{-4} + 4.02 \times 10^{-6}(g_L + 0.1)^{-5} \quad [25]$$

The exponent in Eq. [25] was arrived at by trial and error so that C_2 approaches a constant value for $g_L > 0.4$ as indicated by the data of Murakami *et al.*[8] This procedure, of course, is arbitrary, although the increase of C_2 with a decrease in g_L is qualitatively explainable. With C_2 given by Eq. [25], the average deviation for the set of 67 data is 35 pct, which is very comparable to the average deviation given by the multilinear regression of Eq. [7] or by assuming the Hagen-Poiseuille law as in Eq. [20].

It could be argued that the volume fraction of solid is related to the cube of the characteristic dimension, *i.e.*,

$$(1 - g_L) = (D/d_1)^3. \quad [26]$$

Then if Eq. [26] is used, rather than Eq. [23], the permeability is

$$K = C_2\frac{d_1^2 g_L^3}{(1 - g_L)^{4/3}}; \quad [27]$$

however, the final outcome is no better (as measured by the average percent deviation) than that obtained by combining Eqs. [23] and [24].

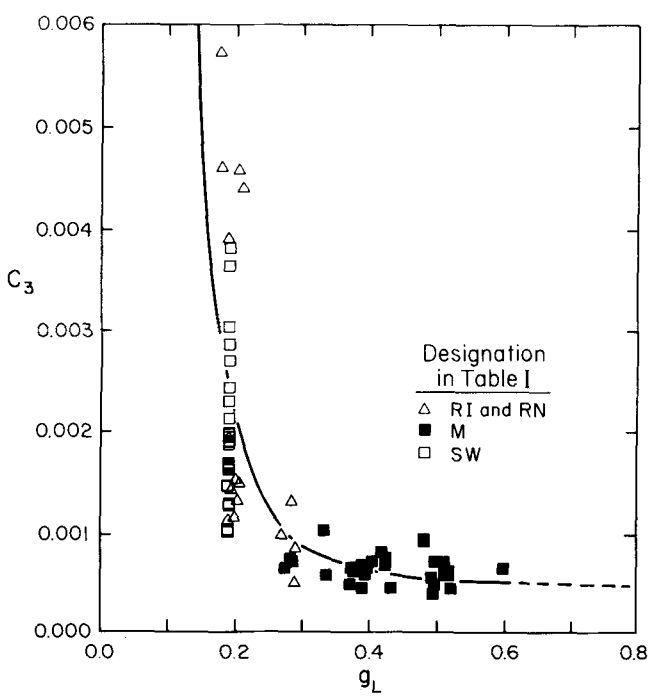

Fig. 3—The parameter C_3, Eq. [24], used in the Blake-Kozeny model to describe flow parallel to the primary dendrite arms.

IV. FLOW NORMAL TO THE PRIMARY DENDRITE ARMS

A. *Multilinear Regression*

When the three-dimensional regression analysis for Eq. [6] was applied to all 43 data of Table II for normal flow, it became apparent that designations RN-DD and RN-Y2 (with the two lowest permeabilities) should not be included because they exhibited abnormally high deviations (>500 pct) with the measured values much less than the calculated values. This was true regardless of the model tested. Therefore these two data are excluded from all results of regressions reported in this section and the following sections.

When the remaining 41 data are subjected to the multilinear regression the result is

$$K = 9.66 \times 10^{-18}\, d_1^{0.699} d_2^{2.73} g_L^{3.34} \quad (\pm 30 \text{ pct}); \quad [28]$$

the result for the set of 29 data for borneol-paraffin is

$$K = 13.13 \times 10^{-19}\, d_1^{1.25} d_2^{2.42} g_L^{3.17} \quad (\pm 16 \text{ pct}), \quad [29]$$

with K in m^2 and d_1 and d_2 in μm. The permeabilities calculated with Eq. [28] are compared to the experimental values in Figure 4.

When either the secondary or primary arm spacing is not included in the regressions, all data sets consistently exhibit average deviations which are somewhat greater than those given by Eqs. [28] or [29], respectively. For example, the respective counterparts to Eqs. [28] and [29] are

$$K = 7.08 \times 10^{-16}\, d_1^{2.08} g_L^{3.32} \quad (\pm 43 \text{ pct}), \quad [30]$$

and

$$K = 3.47 \times 10^{-19}\, d_1^{4.38} g_L^{3.45} \quad (\pm 35 \text{ pct}). \quad [31]$$

These results indicate that, for flow normal to the primary dendrite arms, the secondary dendrite arm spacing is an important variable, at least according to the empirical model represented by the form of Eq. [6].

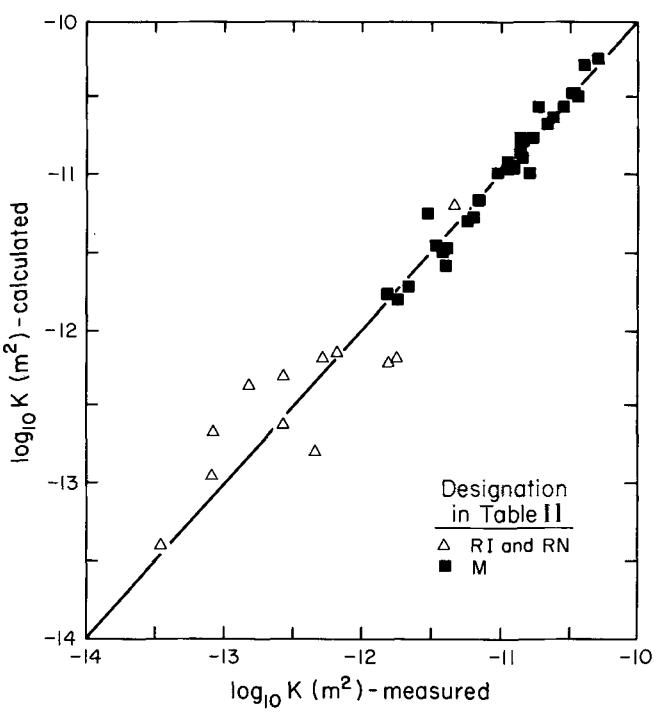

Fig. 4—Measured and calculated permeabilities, Eq. [28], for flow normal to primary dendrite arms.

B. *Slit Model*

With the flow perpendicular to the primary dendrite arms, the model of axial flow through tubes loses its physical meaning. However, the situation can be modeled as flow through "slits" formed by adjacent and parallel primary dendrite arms. Then depicting flow in a slit, the velocity is

$$v = -\frac{\delta^2}{3\mu}\left(\frac{dP}{dy} - \rho g\right) \quad [32]$$

where δ is the semithickness of the slit. The volume flow rate through n flow channels can be expressed as either

$$Q = n(2\delta W)v \quad [33]$$

or as Eq. [13] where W is the width of the "slit", and $2\delta W$ is the cross-sectional area of one flow channel. Then by eliminating Q from Eqs. [13] and [33], we have

$$2\delta W = g_L(n/A)^{-1} \quad [34]$$

where A is the total area of the solid-liquid mixture. The primary dendrite arm spacing in this situation is

$$d_1 = L/n \quad [35]$$

or

$$d_1 = (1/W)(A/n) \quad [36]$$

where L is the distance over which n primary dendrite arms exist and $A = LW$. Then by combining Eqs. [32], [34], and [36], the velocity in a "slit" (*i.e.*, the interdendritic space) is

$$v = -\left(\frac{1}{12}\right)\left(\frac{g_L^2 d_1^2}{\mu}\right)\left(\frac{dP}{dy} - \rho g\right),$$

and by comparing to D'Arcy's law, Eq. [18], the permeability is

$$K = C_3 d_1^2 g_L^2.$$

The form of the equation is the same as that obtained for flow parallel to the primary dendrite arms using the Hagen-Poiseuille law for flow through tubes.

Assuming that an average value of $C_3(3.45 \times 10^{-4})$ applies, the average deviation is more than 200 pct so that this model is not realistic. It can be improved by assuming that C_3 depends upon g_L; with K and d_1^2 in m^2 a regression gives

$$C_3 = -2.82 \times 10^{-5} + 9.90 \times 10^{-4} g_L, \quad [37]$$

but the sample index of correlation is only 0.664. Then when Eq. [37] is combined with Eq. [19], the average deviation is 102 pct, which is still unacceptable and much greater than the average deviation obtainable by the empirical multilinear regression analysis.

The multilinear regression analysis of the previous section suggested that permeability depends strongly on the secondary dendrite arm spacing (d_2). In an attempt to incor-

porate d_2 into this model, C_3 was assumed to vary with d_2. This procedure proved to be fruitless because it gave a result with a greater average deviation than that of Eq. [37]. It is concluded that this model is not suitable for flow normal to the primary dendrite arms.

C. *Crossflow Model*

The pressure drop for flow perpendicular to a bank of very long cylinders[14] is

$$\Delta P = fN\rho v^2/2 \qquad [38]$$

where f = friction factor,
N = number of tubes,
ρ = density of the fluid, and
v = average velocity of the fluid through the area between the tubes.

This flow is illustrated by Figure 5.

For small Reynolds number (Re), the friction factor is inversely proportional to Re so that

$$f = B\mu/Dv\rho \qquad [39]$$

where B is a constant which depends on the arrangement of the tubes and the ratio S/D, D is the tube diameter, and S is the distance between tube centers. Then by combining Eqs. [38] and [39], the average velocity between tubes is

$$v = (2D/B\mu)(\Delta P/N). \qquad [40]$$

In the context of flow of the interdendritic liquid normal to a bank of primary dendrite arms, the primary dendrite arm spacing is

$$d_1 = N/\Delta x \qquad [41]$$

where Δx is the length of the solid-liquid mixture in the flow direction. Also, if n equals the number of tubes (*i.e.*, primary dendrite arms) in an area, A, then

$$1 - g_L = n\pi D^2/4A$$

so that

$$D = (4/\pi)^{1/2}(1 - g_L)^{1/2} d_1. \qquad [42]$$

By combining Eqs. [40] through [42], the velocity of the interdendritic liquid is

$$v = (4/\pi^{1/2}B)(1 - g_L)^{1/2}(d_1^2/\mu)\frac{\Delta P}{\Delta x}; \qquad [43]$$

then a comparison to D'Arcy's law gives the permeability as

$$K = C_4 d_1^2 (1 - g_L)^{1/2} g_L. \qquad [44]$$

In the situation involving a bank of tubes, B increases with increasing values of D/S. Thus according to this model, C_4 should increase with an increase of g_L; this behavior is shown in Figure 6.

With K and d_1^2 in m^2 the curve shown in Figure 6 is

$$\log_{10} C_4 = -2.70 - 0.390 g_L^{-1}, \qquad [45]$$

which gives an average deviation of 41 pct between the measured and calculated values of K.

Because the flow is perpendicular to the primary dendrite arms, it could be rationalized that C_4 would depend on the secondary dendrite arm spacing. Thus regressions were performed on a modification of Eq. [45], giving the result:

$$\log_{10} C_4 = -3.03 - 0.455 g_L^{-1} + 0.82(d_1/d_2). \qquad [46]$$

The ratio d_1/d_2 was selected as a variable in order to make Eq. [46] dimensionally correct. The improvement in terms of the average deviation between the measured and calculated values of K by using Eq. [46] *vs* Eq. [45] is modest (*viz.*, 34 pct *vs* 41 pct, respectively). Thus, the secondary dendrite arm spacing is probably an important variable in this model for flow normal to the primary dendrite arm.

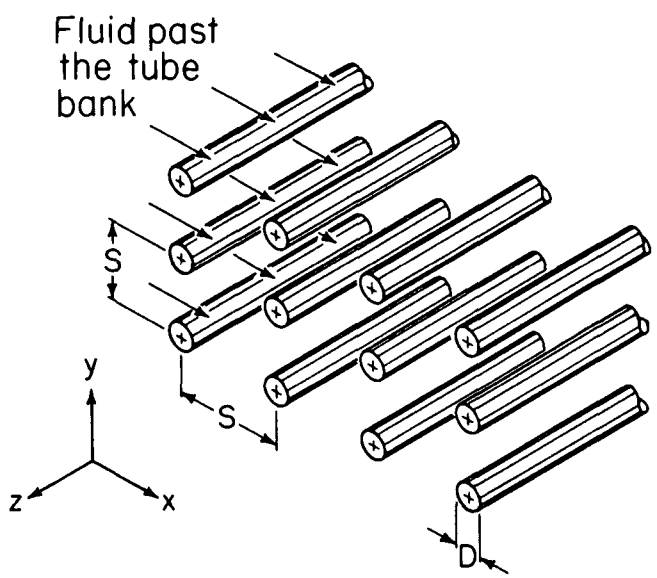

Fig. 5—Flow of liquid perpendicular to a bank of cylinders.

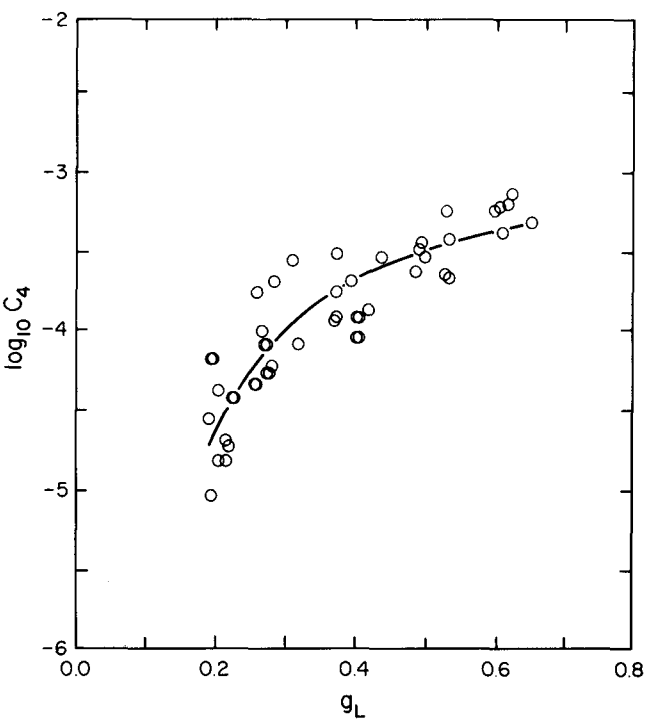

Fig. 6—The parameter, C_4, used in the cross-flow model, Eq. [44].

D. *Blake-Kozeny Model*

Various evaluations for the characteristic dimension, D, were substituted into Eq. [22]. The substitutions for the characteristic dimension were

$$1 - g_L = b(D/d)^m \qquad [47]$$

where b = constant, m = 1, 2, or 3, and $d = d_1$, d_2, or $\sqrt{d_1 d_2}$. When Eq. [47] is substituted into Eq. [22], the permeability is

$$K = C_5 d^2 g_L^3/(1 - g_L)^n \qquad [48]$$

where n = 0, 1, or ⅓ for m = 1, 2, or 3, respectively. With the nine combinations, the average deviation varied from 49 pct to 60 pct. The best results were obtained with $d = \sqrt{d_1 d_2}$, and little sensitivity to the value of n was detected. Of the nine combinations, the best result was obtained with n = 0 and

$$C_5 = 2.25 \times 10^{-3} + 2.60 \times 10^{-3} g_L , \qquad [49]$$

although almost equivalent results were generated with n = 1 and n = 3. Equation [49] is applicable when K and d_1^2 in Eq. [48] are expressed in m^2.

A supposed advantage of the Blake-Kozeny model is that it is a physical model, but, even so, to apply the Blake-Kozeny equation it is necessary to relate the characteristic dimension, D, to the volume fraction of liquid and an appropriate dendrite arm spacing, as, for example, by Eq. [47]. Thus, some arbitrariness is introduced into the Blake-Kozeny model detracting from its advantage as a physical model.

The rationale for Eq. [47] is that the volume fraction of the solid, $1 - g_L$, is proportional to the lineal ratio (m = 1), the areal ratio (m = 2), or the volumetric ratio (m = 3) of the characteristic dimension of the solid, D, to the dimension which defines the space associated with a dendrite arm, d. Whether m = 1, m = 2, or m = 3 is not evident, but it is reasonable to assume that $1 \le m \le 3$ so that n should satisfy $0 \le n \le ⅓$ in Eq. [48]. d can be looked upon as a characteristic dendrite spacing related to both d_1 and d_2. To maintain the correct dimensions for Eq. [48], it is assumed that

$$d = d_1^p d_2^{2-q} . \qquad [50]$$

With Eq. [50], Eq. [48] becomes:

$$K = C_5 (d_1/d_2)^p d_2^2 g_L^3 (1 - g_L)^{-n} . \qquad [51]$$

Values of p and n were determined by a two-dimensional, multilinear regression analysis that gave the following result:

$$K = 1.73 \times 10^{-3} (d_1/d_2)^{1.09} d_2^2 g_L^3 (1 - g_L)^{-0.749} \quad (\pm 43 \text{ pct}) \qquad [52]$$

with K in m^2 and d_1 and d_2 in m. This result indicates that both of the dendrite arm spacings are important with $d \sim (d_1 d_2)^{1/2}$. Notice, also, that the value of n is in the expected range.

V. DISCUSSION

To apply the results presented herein, it is important to decide which model or regression analysis applies best to the data, in terms of a figure of merit (*e.g.*, the average percent deviation between the measured and calculated permeabilities). But it should also be recognized that the results are likely to be extrapolated beyond the scope of the volume fraction liquid represented in Tables I and II. Specifically consider the three equations for describing the normal permeability that are shown in Figures 7 and 8. In Figure 7 the primary and secondary dendrite arm spacings are presumed to be 300 and 125 μm, respectively, and in Figure 8 they are 100 and 40 μm, respectively.

For the example of the larger dendritic spacings, Figure 7, it can be seen that the three models (curve A — the multilinear regression, B — the crossflow model, and C — the Blake-Kozeny model) give comparable results for volume fractions of liquid within the scope of the experiments ($0.19 < g_L < 0.66$). For the smaller dendritic spacings, and again for the experimental scope of g_L, the agreement between curves B and C is very good, but the multilinear regression (curve A) gives permeabilities that are substantially less than those obtained from curves B and C.

Perhaps of more interest are the extrapolations shown in Figures 7 and 8. The crossflow model is unrealistic because $K \to 0$ as $g_L \to 1$ in the vicinity of $g_L = 1$. The most realistic behavior is such that $K \to \infty$ as $g_L \to 1$ as shown by the Blake-Kozeny model (the curves C in Figures 7 and 8). Actually, K should approach a value consistent with flow in an open channel, but that value is at least several orders of magnitude greater than the greatest value of K shown in Figures 7 and 8. Curve B, representing the multilinear regression, gives a finite value for permeability as $g_L \to 1$. Thus, from this point of view, the best model for representing the normal permeability is based upon the Blake-Kozeny equation, even though the average deviations between the measured and calculated values of normal permeability for $0.19 < g_L < 0.66$ are less for the crossflow model and for the multilinear regression.

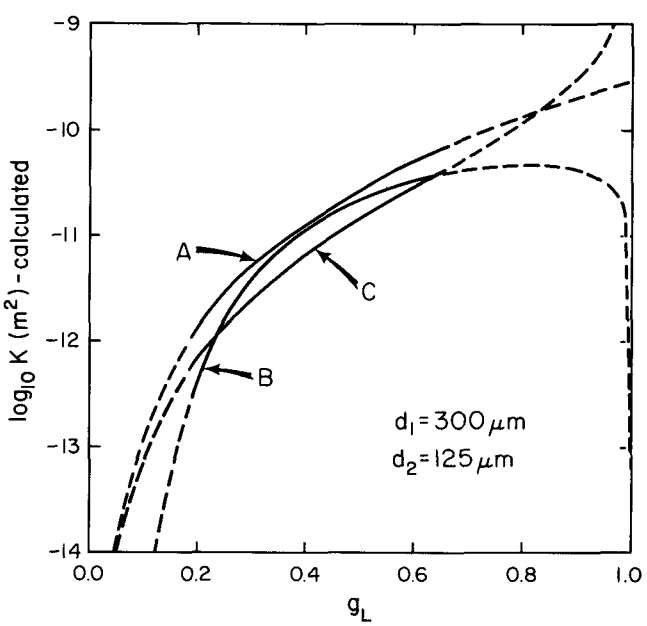

Fig. 7 — Comparisons of equations for permeability when flow is normal to primary dendrite arms: A is calculated with Eq. [27]; B is calculated with Eqs. [43] and [45]; C is calculated with Eq. [51]. Broken curves indicate extrapolations beyond the range of available data.

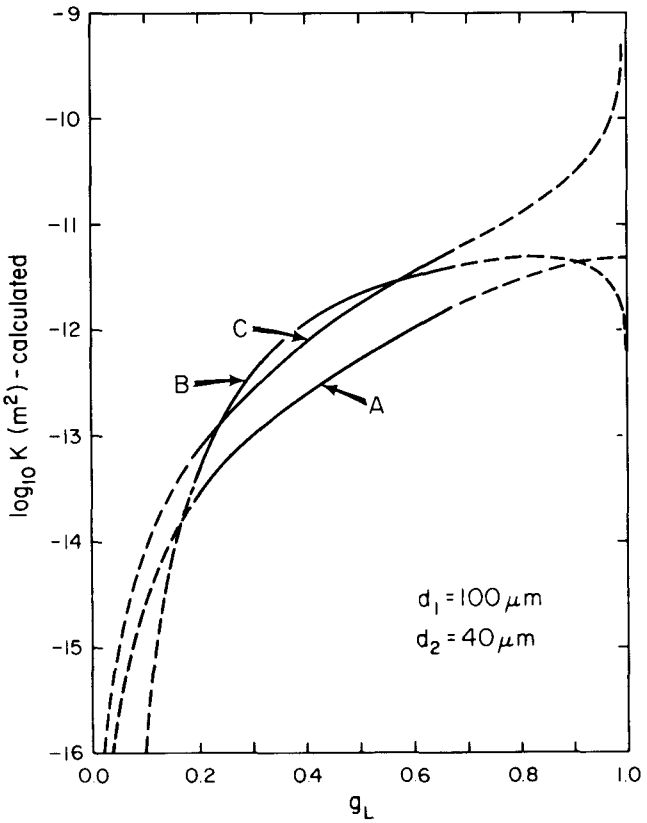

Fig. 8 — Comparison of equations for permeability when flow is normal to primary dendrite arms: A, B, and C as in Fig. 7.

Examples similar to Figures 7 and 8 are not shown for parallel permeability, but based upon the same argument the Blake-Kozeny model is more appropriate than is the Hagen-Poiseuille model for extrapolating beyond the scope of the experimental values of g_L.

Finally, Figures 9 and 10 are presented to show the ratio of the parallel permeability to the normal permeability. This ratio should approach unity as $g_L \rightarrow 1$. If the equations with the least values of the average deviation between measured and calculated permeabilities are selected (Figure 9), then the ratio behaves properly as $g_L \rightarrow 1$ for the example of the lesser dendritic spacings if allowance is made for the "scatter" in the equations used to calculate the permeabilities. However, the ratio is only 0.22, at the most, for $g_L = 1$ for the example of the larger dendritic spacings. On the other hand, when the Blake-Kozeny model is selected for both the parallel and normal permeabilities, as in Figure 10, the values of the ratio of the permeabilities do bracket unity for $g_L = 1$ if allowance is made for the scatter.

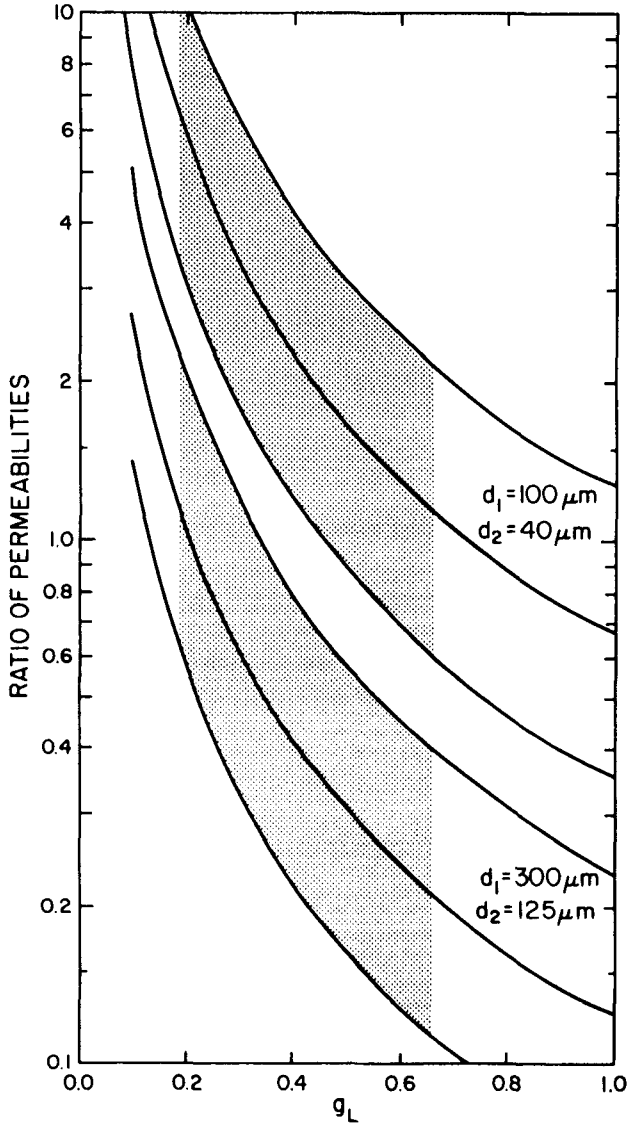

Fig. 9 — Ratio of permeabilities as computed with Eqs. [20] and [27]. The shading indicates the range of experiments on which the results are based.

VI. CONCLUSIONS

1. Within the scope of the experimental values of volume fraction liquid, $0.17 < g_L < 0.61$, the permeability data for parallel flow are represented best by the Hagen-Poiseuille model, Eq. [20].
2. Within the scope of the experimental values of volume fraction liquid, $0.19 < g_L < 0.66$, the permeability data for normal flow are represented best by a multilinear regression, Eq. [28].
3. When flow is parallel to the primary dendrite arms, the permeability depends upon d_1 but not d_2.
4. When flow is normal to the primary dendrite arms, the permeability depends upon both d_1 and d_2.
5. When it is necessary to extrapolate beyond the scope of the experimental values of g_L, equations based upon the Blake-Kozeny model are recommended. Specifically Eqs. [24] and [25] are recommended for the parallel permeability, and Eq. [52] is recommended for the normal permeability.

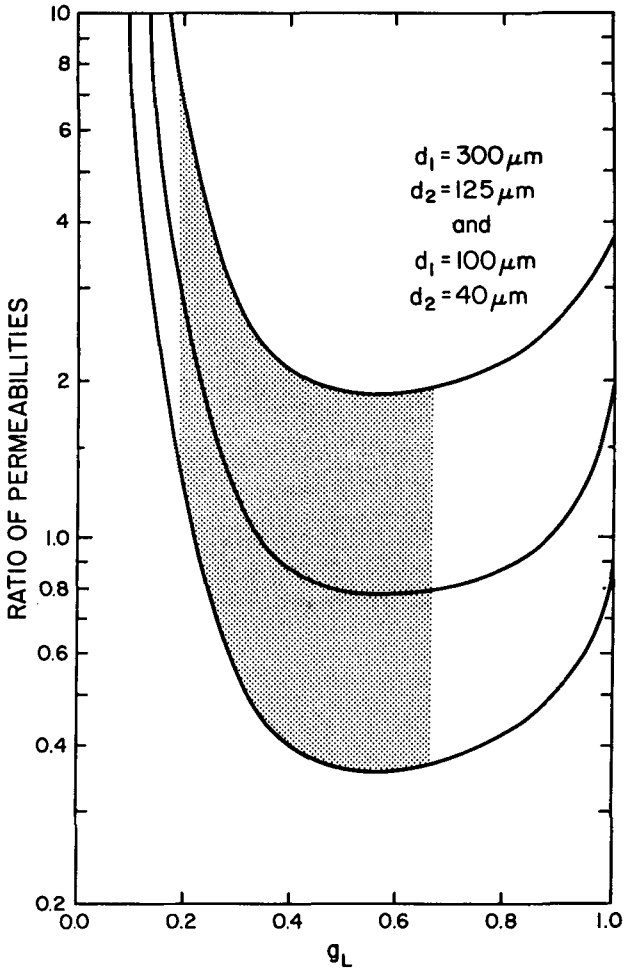

Fig. 10—Ratio of permeabilities as computed with Eq. [51] and Eqs. [24] and [25]. The shading indicates the range of experiments on which the results are based.

ACKNOWLEDGMENTS

This work was sponsored by the National Science Foundation (Grant DMR-820554). R. Inturi, formerly at the University of Arizona (U.A.) and now at The Ohio State University, performed many of the permeability experiments. Dr. K. Yeum (U.A.) was invaluable because he shared his expertise in computer software, graphics, and data management. Quantitative metallography was done by V. Koegel (U.A.) and by A. Studer and Dr. V. Laxmanan at the Lewis Research Center (NASA). Also, the author has had extensive discussions with D. Koegel, R. Nasser-Rafi, and R. Deshmukh, all co-workers during the period of the grant. For all of this assistance, I am very grateful.

REFERENCES

1. T. S. Piwonka and M. C. Flemings: *TMS-AIME*, 1966, vol. 236, pp. 1157-65.
2. D. Apelian, M. C. Flemings, and R. Mehrabian: *Metall. Trans.*, 1974, vol. 5, pp. 2533-37.
3. N. Streat and F. Weinberg: *Metall. Trans. B*, 1976, vol. 7B, pp. 417-23.
4. T. Takahashi: U.S.-Japan Cooperative Science Program Seminar on Solidification Processing, Dedham, MA, June 26-29, 1983, National Science Foundation (USA) and Japan Society for Promotion of Science, pp. 45-60.
5. K. Murakami and T. Okamoto: *Acta Metall.*, 1983, vol. 31, pp. 1741-44.
6. R. Nasser-Rafi, R. Deshmukh, and D. R. Poirier: *Metall. Trans. A*, 1985, vol. 16A, pp. 2263-71.
7. K. Murakami, A. Shiraishi, and T. Okamoto: *Acta Metall.*, 1983, vol. 31, pp. 1417-24.
8. K. Murakami, A. Shiraishi, and T. Okamoto: *Acta Metall.*, 1984, vol. 32, pp. 1423-28.
9. H. Abrams: *Stereology and Quantitative Metallography*, ASTM STP 504, American Society for Testing and Materials, 1972, pp. 138-82.
10. Multilinear Regression, Dynacomp, Inc., Rochester, NY, 1980.
11. G. H. Geiger and D. R. Poirier: *Transport Phenomena in Metallurgy*, Addison-Wesley, Reading, MA, 1973, p. 45.
12. G. H. Geiger and D. R. Poirier: *Transport Phenomena in Metallurgy*, Addison-Wesley, Reading, MA, 1973, p. 94.
13. G. H. Geiger and D. R. Poirier: *Transport Phenomena in Metallurgy*, Addison-Wesley, Reading, MA, 1973, p. 43.
14. B. V. Karlekar and R. M. Desmond: *Engineering Heat Transfer*, West Publishing Co., St. Paul, MN, 1977, pp. 321-24.